Check for updates

ADVANCED ELECTRONIC MATERIALS
www.advelectronicmat.de

Low-Pressure Mechanical Switching of Ferroelectric Domains in $PbZr_{0.48}Ti_{0.52}O_3$

Gaurav Vats, Ravikant, Peggy Schoenherr, Ashok Kumar,* and Jan Seidel**

Low-energy switching of ferroelectrics is currently being investigated for energy-efficient nanoelectronics. While conventional methods employ electrical fields to switch the polarization state, mechanical switching is investigated as an interesting alternative low-energy switching concept, if low enough pressures could be achieved. Here, the thickness-dependent mechanical and electrical switching behavior of ferroelectric $PbZr_{0.48}Ti_{0.52}O_3$/$YBa_2Cu_3O_{7}$_δ (PZT/YBCO) epitaxial heterostructures grown on single crystalline $LaAlO_3$-$(001)_{\text{pseudo-cubic}}$ (LAO) substrate is reported. Mechanical switching is found under relatively low force (600 nN; estimated pressure ≈0.21 GPa) in atomic force microscopy-based measurements. Mechanically switched domains can be erased by small electric fields and, interestingly, exhibit a surface potential change similar to electrically poled areas. The feasibility of switching these heterostructures with very low pressure makes them promising candidates for nanoscale electromechanical devices.

Mechanical control of ferroelectric domains[1] is a less explored phenomenon in contrast to more conventional electrical and optical switching.[2,3] Scientific reports on various aspects of mechanical switching of ferroelectric domains suggest that the mechanically switched domains in ferroelectrics could either occur individually or by the cumulative effect of the several mechanisms[4] including flexoelectric effect,[1] ferroelectric–ferroelastic switching[5,6] and chemical modifications on the surface[7] and in the bulk.[8,9] The electrochemical effect in the bulk can be induced by diffusion of oxygen vacancies,[10] which in turn can lead to electrostatic or Vegard strain.[4] The contribution of the aforementioned mechanisms in depicting mechanical switching of ferroelectrics has been discussed recently,[4,11] while further work is still required to gain a more complete understanding. Scanning probe-based investigations of mechanical behavior in ferroelectrics,[12] especially localized mechanical writing of nanoscale domains and mechanical erasing of electrically written domains[1] provide a suitable platform for further investigation of mechanoelectric devices[13,14] and concepts.[15,16] Ultralow pressure mechanical writing and noncontact reading might lead to new low energy electronics concepts and information storage energy costs of attojoule/bit, which has been explored for example through electrical control of magnetism concepts.[17]

Mechanical switching has been reported in a range of ferroelectric materials from single crystals ($BaTiO_3$,[18] $(1-x)Pb(Mg_{1/3}Nb_{2/3})O_3 - xPbTiO_3$ ($x = 0.32, 0.40$)[19]) to thin films ($(Pb(Zr_{0.2}Ti_{0.8})O_3$,[20,21] $BaTiO_3$,[1,22] $BiFeO_3$[23–25]). Among these, $Pb(Zr_{0.2}Ti_{0.8})O_3$ thin films have shown promising mechanical switching properties with anticipated memory storage capacities of the order of 110 Gb cm^{-3} reported using atomic force microscope (AFM) tip forces down to 300 nN.[20] Such tip force leads to an estimated pressure of 3.8 GPa with a tip radius of 5 nm under the assumption that the tip-sample contact is represented by a disc of radius equivalent to the tip radius.[1,26] This pressure is considerably lower than the reported values in one of the first studies on mechanical writing of ferroelectric domains in $BaTiO_3$.[1] In a related attempt Edwards et al.[6] reported the mechanical switching threshold (1000 nN: estimated tip pressure = 0.8 GPa; tip radius = 20 nm) of polycrystalline $PbZr_{0.53}Ti_{0.47}O_3$, which lays at the morphotropic phase boundary (MPB) of the $Pb(Zr_xTi_{(1-x)})O_3$ family. Compositions close to the MPB of $Pb(Zr_xTi_{(1-x)})O_3$ offer the possibility of transitions between tetragonal and rhombohedral phases due to small strains[27–31] as well as the co-existence of tetragonal and rhombohedral phases,[5,32] and have been investigated with respect to thickness-dependent flexoelectric fields,[32] making them ideal for pressure-induced polarization switching. Therefore, in this work, we explore the ferroelectric and mechanical

---

Dr. G. Vats, Dr. P. Schoenherr, Prof. J. Seidel
School of Materials Science and Engineering
University of New South Wales
Sydney, NSW 2052, Australia
E-mail: g.vats@unswalumni.com; jan.seidel@unsw.edu.au

Prof. Ravikant, Dr. A. Kumar
CSIR-National Physical Laboratory
Dr. K. S. Krishnan Marg, Delhi 110012, India
E-mail: ashok553@nplindia.org

Prof. Ravikant, Dr. A. Kumar
Academy of Scientific and Innovative Research (AcSIR)
Ghaziabad 201002, India

Prof. Ravikant
Department of Physics
Government College Sailana
Vikram University
Ujjain, Madhya Pradesh 456010, India

Dr. P. Schoenherr, Prof. J. Seidel
ARC Centre of Excellence in Future Low-Energy Electronics Technologies
UNSW Sydney
Sydney, NSW 2052, Australia

The ORCID identification number(s) for the author(s) of this article can be found under https://doi.org/10.1002/aelm.202000523.

DOI: 10.1002/aelm.202000523

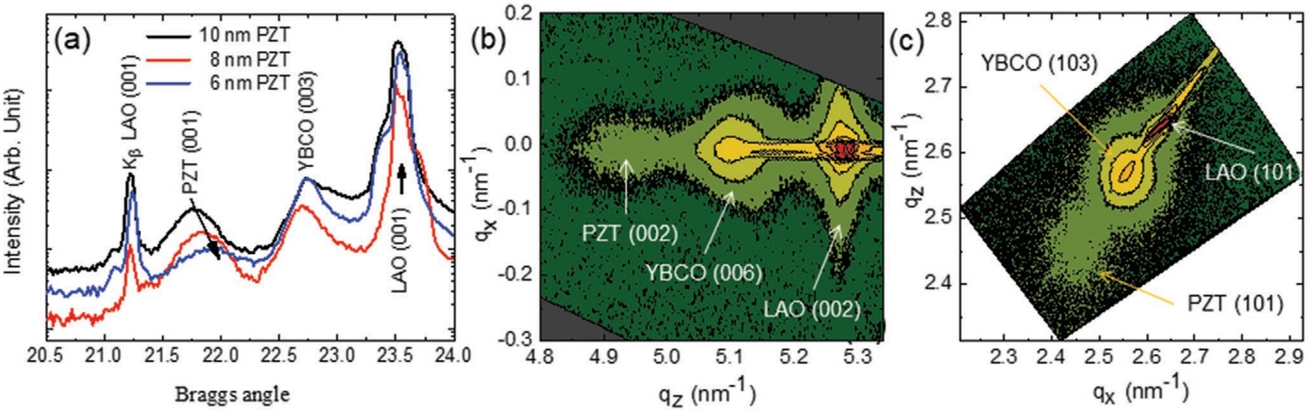

Figure 1. Structural characterization. a) X-ray diffraction patterns of the PZT/YBCO/LAO heterostructures with PZT thickness of 6 nm (S1), 8 nm (S2), and 10 nm (S3). Reciprocal space maps (RSM) of S2 around the b) (002) and c) (101) reflection of the LAO substrate.

switching properties of epitaxially grown $PbZr_{0.48}Ti_{0.52}O_3$ (PZT) thin films on $YBa_2Cu_3O_{7-}\delta$ (YBCO), where PZT is a member of the MPB $Pb(Zr_xTi_{(1-x)})O_3$ family.

Figure 1a shows the room temperature (297 K) HR-X-ray diffraction (XRD) patterns of the PZT/YBCO/LAO heterostructures. The high-resolution X-ray diffraction (HR-XRD) data shows two peaks at 21.3° and 23.6° corresponding to LAO (001), one broad peak belonging to PZT (001) and another one to YBCO (003). The absence of Bragg planes other than 00*l* confirms the unidirectional crystal growth of the as-grown heterostructures. A substantial shift in the broad PZT (001) peaks toward higher Bragg angles with decreasing PZT film thickness is observed, which may be due to an enhanced out-of-plane compressive strain and in-plane tensile strain.[33] It has been reported that twin domains in the LAO substrate (evident from a shoulder in the LAO XRD peak as seen for Samples S1–S3 in Figure 1a can cause a variation in the lattice strain and properties of the top YBCO layer.[34] This is also likely to influence the properties of the PZT layers deposited on YBCO.

The out-of-plane compressive strain (ε) is defined by the equation[33]

$$\varepsilon = \frac{c_{\text{film}} - c_{\text{bulk}}}{c_{\text{bulk}}} \tag{1}$$

with c_{film} and c_{bulk} being the PZT film and PZT bulk out-of-plane lattice constant, respectively (c_{bulk} is calculated from XRD of the PZT target; not shown here). The strain values are summarized in **Table 1**. It is found that the out-of-plane compressive strain on PZT decreases with an increase in film thickness.

Table 1. Calculated out-of-plane compressive strain in PZT/YBCO/LAO heterostructures.

PZT film thickness [nm]	Bragg angle [°]	c_{bulk} [Å]	c_{film} [Å]	$c_{\text{film}}-c_{\text{bulk}}$ [Å]	$\varepsilon \times 100$
6	21.92	4.140	4.055	−0.085	−2.0
8	21.84	4.140	4.070	−0.070	−1.7
10	21.78	4.140	4.081	−0.059	−1.4

Further detailed analysis of the epitaxial relationship in PZT/YBCO and YBCO/LAO is performed using reciprocal space mapping (RSM) data. Figure 1b,c shows the RSM images for S2 in the symmetric and asymmetric direction along the LAO (002) and (101) orientation. The RSM data along the (002) direction reveals the growth direction along the *c*-axis (perpendicular to the substrate surface). The three observable reciprocal points belong to PZT (002), YBCO (006), and LAO (002), respectively (Figure 1b left to right). From these reciprocal points, the out-of-plane *c* lattice parameter is determined as 4.050 and 11.759 Å corresponding to PZT and YBCO, respectively. This PZT value is close to the out-of-plane lattice parameters calculated from the θ–2θ XRD data for S2 (Table 1). In the case of the asymmetric scan (Figure 1c), two reciprocal points other than the substrate with *q* vectors 2.456 nm^{-1} (4.066 Å) and 2.558 nm^{-1} (3.797 Å) are assigned to the PZT (101) and YBCO (103) planes, respectively. The presence of symmetric and asymmetric reciprocal points in the RSM data[35] confirms the epitaxial nature of our PZT/YBCO films on LAO.

To investigate the mechanically induced nanoscale ferroelectric switching behavior of the PZT/YBCO/LAO heterostructures, we firstly perform electrical poling experiments and image the ferroelectric domains using PFM. **Figure 2**a–c depicts a typical polarization reversal experiment where the dark and bright areas correspond to a downward and upward polarization, respectively. As grown polarization of Samples S1 and S2 switch with a tip voltage of +3 V and S3 with a voltage of −2 V. We mostly detect a full reversal of polarization in all three films (180° phase change in the PFM image; see Section S1.1 in the Supporting Information). Additionally, the in-plane signals (Figure S1.2j–o, Supporting Information) are rather weak, likely because of the very small thickness of the films and a predominantly out-of-plane polarization. The area outside the poled boxes in Figure 2a–c corresponds to the polarization direction of the as-grown PZT. In PZT films below 8 nm, the as-grown polarization direction is "up" (i.e., pointing out of the surface), while it is pointing "down" for the 10 nm film (S3). A reversal of as-grown polarization direction dependent on film thickness has also been found in other reports on ferroelectric heterostructures, including MPB members of $Pb(Zr_xTi_{(1-x)})O_3$[28,32] and BFO.[36,37] In these reports, the reversal is explained by a

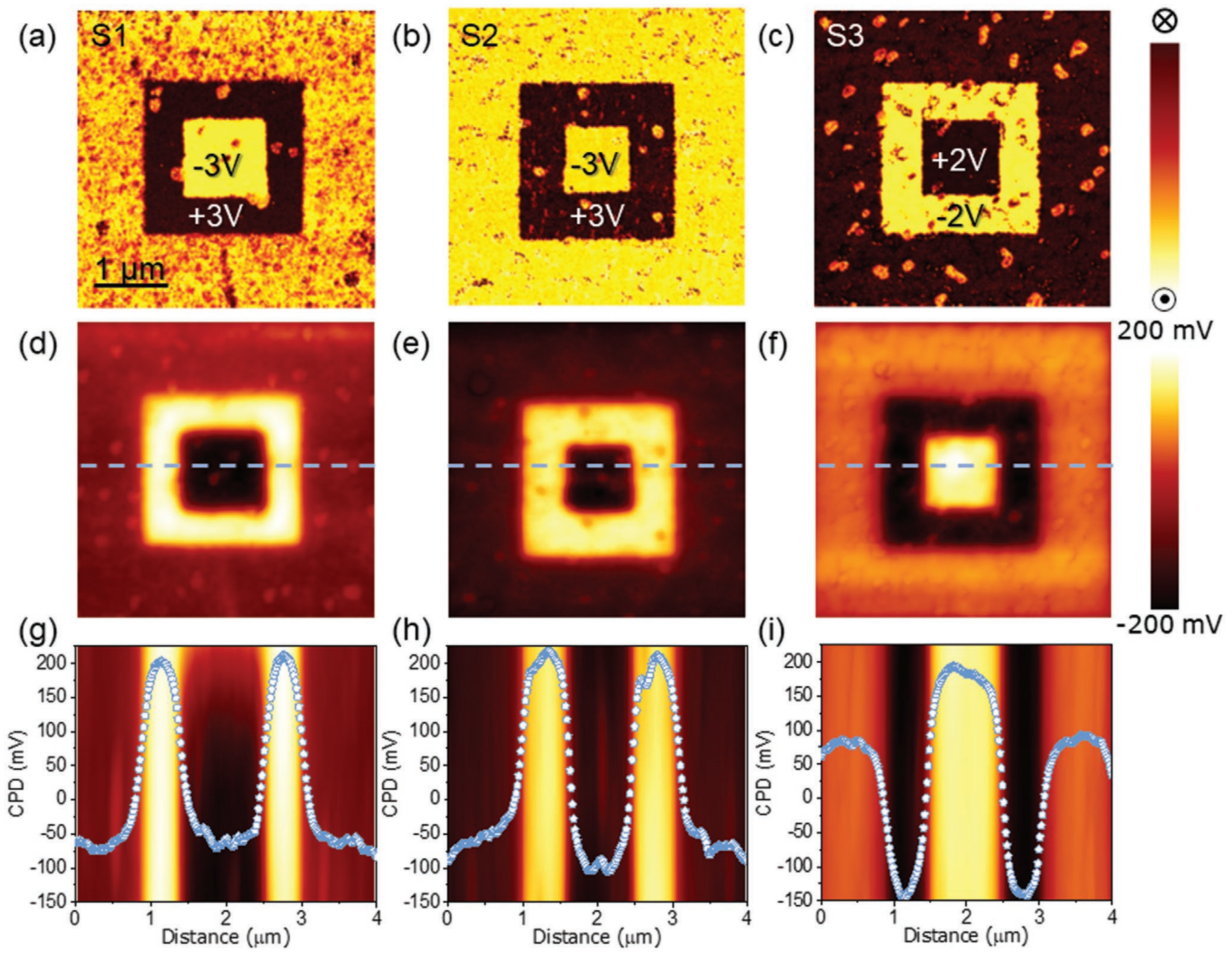

Figure 2. Electrical switching behavior. a–c) PFM phase images, d–f) KPFM images and g–i) line profiles (of blue lines in (d–f)) for Samples S1, S2, and S3, respectively. Two bright orange lines in (f) are artifacts.

competition between a flexoelectric effect induced by the strain in the film and an electric field due to band bending at the interface. Our experiments show an opposite thickness-dependent as-grown polarization than the one detected by Yu et al.[32] on $La_{0.67}Sr_{0.33}MnO_3/PbZr_{0.52}Ti_{0.48}O_3$ heterostructures, which have a Zr/Ti ratio quite close to the composition of our samples. Zr/Ti in our samples is 48/52 which brings them relatively closer to the MPB in the $Pb(Zr_xTi_{(1-x)})O_3$ phase diagram.[38] The difference in the as-grown state of polarization could also result from a different strain in our PZT films and a different bottom electrode.

In order to quantify the strain gradients in our films, we performed Williamson–Hall analysis[39] (see Note S1 and the corresponding figure in the Supporting Information). The highest (0.44%) inhomogeneous strain (ε_i) is found for the 10 nm film followed by 0.30% in 6 nm and 0.25% in 8 nm films. The inhomogeneous strain values were used to calculate the strain gradients $\left(\frac{\partial u_i}{\partial x_i}\right)$[37] followed by an estimate for the flexoelectric field $\left(E_{\text{flexoelectric}} = \frac{\gamma e}{a_i \varepsilon_0} \frac{\partial u_i}{\partial x_i}\right)$.[36] Here, γ is a scaling factor (assumed = 1), e is the charge of one electron, a_j is the lattice constant and ε_0 is the permittivity of the free space. The strain gradients are found to be -15.35×10^5, -11.15×10^5, and -17.34×10^5 m^{-1} in 10, 8, and 6 nm thin PZT films, respectively. The flexoelectric field values in 6, 8, and 10 nm PZT films were found to be 77, 49.5, and 69 MV m^{-1}, respectively. The strain gradients are similar in all films and agree with the reported values of $PbZr_{0.52}Ti_{0.48}O_3$ films with similar thickness.[32] This insinuates that the difference in polarization orientation and reversal compared to ref. [32] is dominated by the interface effect that varies due to different bottom electrodes and our heterostructures.

We investigated the above-mentioned switched areas by contact potential difference (CPD) measurements using Kelvin probe force microscopy (KPFM) with an AFM tip lift height of 40 nm. CPD mapping of the Samples S1, S2, and S3 can be seen in Figure 2d–f. The light yellow color in the KPFM images shows that the CPD is higher in the positively poled areas than in the negatively poled areas. This is due to the screening of electrostatic charges at the tip-sample interface.[40] Thus, the positively poled area is likely to have positive charges accumulated on the PZT surface and vice versa for a negatively poled

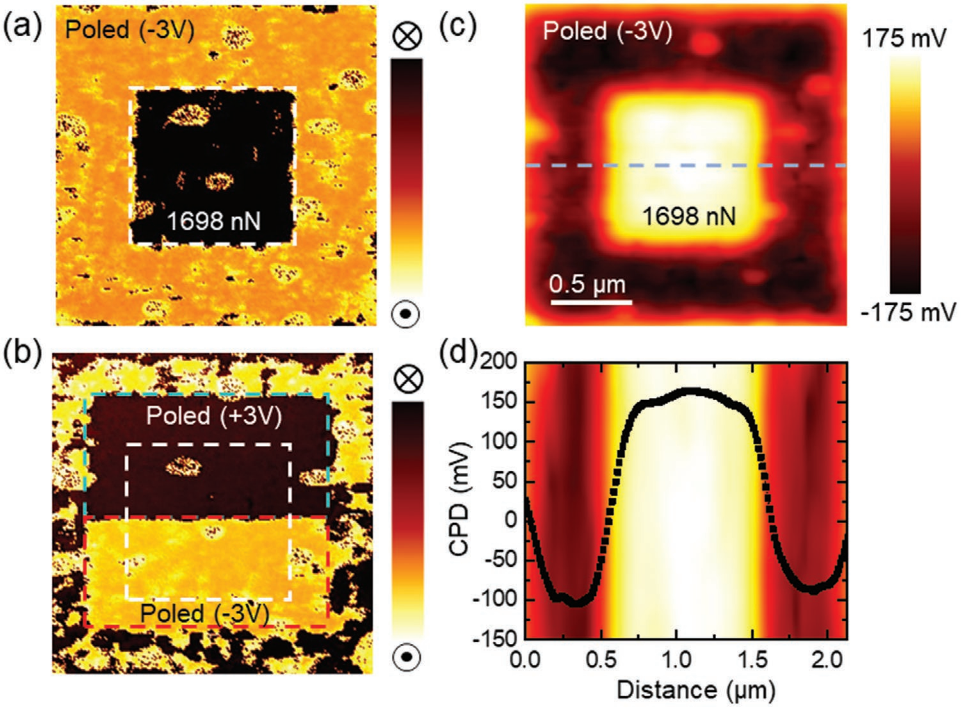

Figure 3. Electromechanical writing and erasing with noncontact reading using AFM. a) Mechanically written domain (shown by white dotted square) with 1698 nN on an electrically poled area with −3 V (sample S2). b) Effect of an electric field (±3 V) on a mechanically written domain (white dotted square). Area poled with −3 V (red dotted box) is found to be capable of erasing mechanically written domains while the area poled with +3 V (cyan dotted box) remains unchanged. c) KPFM mapping and d) CPD line profile of mechanically written domain in the image (a).

area. The magnitude of the accumulated charge depends on the as-grown polarization and the applied switching voltage. CPD values for negatively poled areas are −50, −100, and −150 mV for S1, S2, and S3, respectively (see line profiles in Figure 2g–i). On the other hand, the average CPD values for the areas poled with a positive bias are +200, +210, and +180 mV for S1, S2, and S3, respectively. Note that the negative bias poling (resulting in polarization pointing up) lowers CPD in all cases, but more so for increasing film thickness, which could originate from thickness-dependent changes in the polarization of the films.

After analyzing the electrical switching behavior for samples with different thickness of the PZT layer on YBCO, mechanical switching experiments were performed. All samples showed unidirectional mechanical switching, i.e., upward polarization (bright) is switched downward (dark) as demonstrated in Figure S.2.1 in the Supporting Information. This means that the flexoelectric effect works analogously to an applied positive bias. It has to be noted that the 10 nm PZT sample (S3) has an as-grown downward polarization, which needs to be poled upward with −3 V prior to mechanical switching. **Figure** 3a shows a PFM image of mechanical switching on S2 with a force of 1648 nN exerted by an AFM tip on a prior electrically written domain (tip voltage −3 V). The PFM image in Figure 3a was acquired with an amplitude of 1 V (peak-to-peak) under an intentional low mechanical loading of 97 nN (tip pressure: 0.03 GPa) to avoid further mechanical influence during the PFM scan. The bright contrast in the mechanical influenced area shows a polarization reversal toward the substrate. This unidirectional mechanical switching is also found in the other two PZT films (see Section S2.1 in the Supporting Information for a comparison of S1, S2, and S3 films). The exerted tip pressure can be roughly estimated by assuming a disk-shaped contact area of the same size as the tip radius.[26,41–43] In our case this leads to a tip pressure of ≈0.5 GPa (tip radius = 30 nm), although the actual contact area can vary significantly from the AFM tip radius.

In the next step, the mechanically written domain is manipulated with a voltage of ±3 V (see Figure 3b). A consecutive PFM image reveals that a tip voltage of −3 V (dotted red box) erases the mechanically written domain (dotted white square), while +3 V has no impact (dotted cyan box). Thus, it can be concluded that the mechanically induced domains in sample S2 are fully reversible with applied negative bias and behave analogously to domains created with a positive bias.

To further highlight the similarities between the mechanical and electrical poling, Figure 3c shows the KPFM image of the mechanical switched area in Figure 3a. The mechanically switched area exhibits similar, albeit slightly lower CPD change compared to the electrically switched region with positive bias (see Figure 2h). This is highlighted by the line cut of the CPD image in Figure 3d (along the blue line in Figure 3c), which shows a CPD change of nearly 250 mV from the negatively poled area to the mechanically switched region. This indicates that the analog outcomes are generated by mechanical poling as by applying a positive bias. This is only possible if both (electrical and mechanical poling) have a similar impact on the state of polarization. Mechanical switching and KPFM measurements performed on Samples S1 and S3 (Figure S2.2, Supporting Information) show similar results supporting the conclusions made above. However, it is to be noted that sample S3 needs to be first electrically poled with −3 V to observe mechanical switching. This is expected as S2 and S3 have opposite as-grown polarization. Consequently, our PFM, as well as KPFM images, clearly show that mechanical poling/de-poling is possible in PZT/YBCO heterostructures.

Due to the sample composition being close to the MPB, a pressure-induced transition from the tetragonal to the rhombohedral phase or vice versa could also be envisaged to cause such a polarization reversal.[5,6] The application of a mechanical strain has been reported to lead to a change in the in-plane and the out-of-plane response of MPB members of $Pb(Zr_xTi_{(1-x)})O_3$.[5,6] However, these experiments only found polarization changes <90[6] in contrast to the 180° switching found in this report (no in-plane phase or amplitude signal in the PFM measurements could be detected indicating an in-plane polarization below our measuring sensitivity). Another indicator that the polarization reversal in our experiments is not driven by a pressure-induced phase transition is the absence of pressure-induced kinks in the force–distance curves. Such kinks in the force–distance curves have been reported in other ferroelectrics with morphotropic phases to confirm phase transitions.[23,24] However, the pressure of the tip can directly impact the polarization through the ferroelastic mechanism or flexoelectric effect[32] as discussed before. It can also manipulate the local screening charges or induce local shifts in electrochemical potential due to vacancies diffusion.

Flexoelectricity has been reported to play an important role in polarization reversal in thin $Pb(Zr_{0.2}Ti_{0.8})O_3$ films (5–20 nm)[4] and the presence of an in-built flexoelectric field[32] can influence tip-generated flexoelectricity through mechanical loading. Flexoelectric trailing fields[44] have also been reported to influence ferroelastic switching, which can be seen in scanning direction-dependent mechanical switching. This effect can easily be tested as shown in **Figure** 4b, where we mechanically poled S2 with 1400 nN force at different scan angles. The consecutive PFM image shows no difference for different scan directions and thus a mechanical trailing field can be excluded.

To further investigate the mechanical switching mechanism, we studied the force-dependent mechanical switching behavior. Figure 4a,c shows PFM and CPD images of S2 with forces of 600 nN, 800, 1000, 1200, 1400, and 1600 nN. All six force values induce a full polarization reversal with a similar CPD value change (Figure 4d). The CPD values are in accordance with values measured in Figure 3. The observation of nearly similar CPD values for applied forces larger than 600 nN (estimated pressure ≈0.21 GPa) suggests that a force threshold is required to switch the polarization, but more force does not influence the polarization further. Also, especially due to the YBCO bottom electrode, pressure-induced oxygen vacancies diffusion in PZT could have an influence, as YBCO is well known for oxygen vacancies,[45,46] and pressure-induced conductivity[47] changes. Poling of our sample leads to changes in local conductivity, as seen in the c-AFM measurement (see Section S2.3 in the Supporting Information), pointing to the possibility of changes in local oxygen vacancy content as reported in other materials.[48,49] In addition, the delta in our films is between 0.2 and 0.7, as the YBCO was found to be superconducting in other measurements.[50] In addition to its superconducting properties it is also an ideal heterostructure electrode at room temperature.[51-53] Changes of oxygen content, i.e., delta after electrical or mechanical poling are possible, but could not be quantified with available methods in our case. We note that conductive AFM measurements of poled areas show variations of conductivity (Figure S.2.3, Supporting Information), which could be influenced by oxygen content variations. Therefore, favorable epitaxial strain conditions for a tip-induced flexoelectric effect together with potential oxygen vacancy contributions are the most likely reasons for mechanical switching in our films.

In conclusion, this study reports novel $PbZr_{0.48}Ti_{0.52}O_3$/$YBa_2Cu_3O_{7-\delta}$ (PZT/YBCO) epitaxial heterostructures grown on

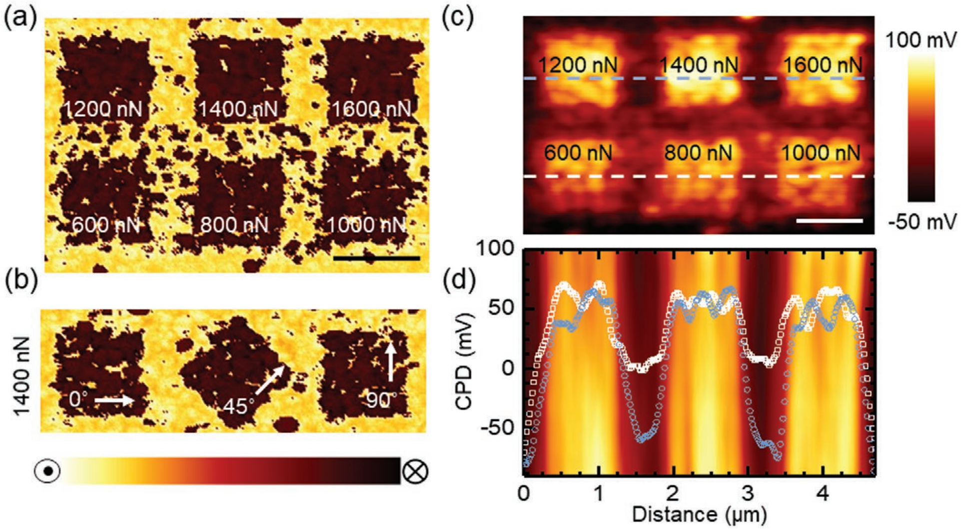

Figure 4. Mechanical writing of ferroelectric domains. a) PFM phase images of mechanically written domains on S2 with different tip force (600 to 1600 nN). b) PFM phase images of mechanical written domains under different scanning angles with an applied force of 1400 nN. c) KPFM mapping and d) line profile of the image (a). (Scale bar = 1 μm)

single crystalline $LaAlO_3$-(001)$_{\text{pseudo-cubic}}$ (LAO) substrate. Thickness dependent electrical switching behavior in 6 nm (S1), 8 nm (S2), and 10 nm (S3) PZT films suggest that it is possible to achieve different as-grown states of polarization by merely controlling the epitaxial strain and film thickness. We found that films exhibit a low pressure (≈0.21 GPa) mechanical switching of the ferroelectric polarization. The depicted switching pressure is significantly lower than previously reported tip pressures used for mechanical switching in $BaTiO_3$.[1] Interestingly, even though the films have different directions of polarization in the as-grown state, the mechanical poling/switching is found to work analogous to an applied positive bias. Low-pressure switching of ferroelectrics without electrical bias presents new opportunities for next-generation low-energy electronics and domain wall electromechanical applications.

Experimental Section

To fabricate PZT/YBCO heterostructures, YBCO and PZT targets were prepared using the conventional solid-state reaction route.[54] Afterward, PZT/YBCO heterostructures were deposited on one-side-polished single-crystalline $LaAlO_3$-(001)$_{\text{pseudo-cubic}}$ (LAO) substrates (Crystal GmbH-company, a = 3.789 Å) using pulsed laser deposition (PLD). Firstly, 100 nm YBCO thin films were deposited as a bottom electrode by using a KrF excimer laser (λ = 248 nm) with an energy density of 1.2 J cm^{-2}, repetition rate 3 Hz and substrate temperature 800° C. During the growth of YBCO, oxygen gas partial pressure was maintained at 160 mTorr. Grown YBCO/LAO thin films were cooled down to 550° C and annealed for 1 h to allow domain recrystallization. Then, the substrate temperature was increased to 650° C and PZT layers with thicknesses of 6 nm (S1), 8 nm (S2), and 10 nm (S3) were deposited at an oxygen partial pressure of 80 mTorr with a laser energy density and repetition rate of 1 J cm^{-2} and 5 Hz, respectively. The grown heterostructures were finally cooled down to room temperature at 20° C min^{-1}. The thickness of the films was measured with a Stylus Profilometer. To analyze the crystal structure and confirm the epitaxial growth throughout all layers, HR-XRD was performed in a parallel beam setting. The HR-XRD measurement was accomplished by using monochromatic Cu-Kα radiation (λ = 1.54 Å) in a co-planar geometry with a horizontal sample stage.

Thereafter, nanoscale measurements were performed to determine the local properties of the PZT/YBCO films using a commercial AIST-NT Smart SPM 1000 room-temperature AFM system in a nitrogen environment. MikroMasch NSC35/Pt tips were used for the electrical poling and KPFM measurements on the electrically poled area. Diamond-coated (spring constant = 28 to 91 N m^{-1}) Si cantilevers (model no. DCP20) were utilized for the mechanical switching and PFM measurements. PFM resonant mode measurements were performed using an AC imaging voltage of 1.0 V (peak-to-peak) with frequencies in the range of 600 to 1200 kHz under a mechanical load of 97 nN. KPFM measurements of the mechanically switched areas were performed using the same diamond tips with a lift height of 40 nm.

Supporting Information

Supporting Information is available from the Wiley Online Library or from the author.

Acknowledgements

G.V. and R. contributed equally to this work. G.V., P.S., and J.S. acknowledge the support from the Australian Research Council (ARC) through Discovery Grants and the ARC Centre of Excellence in Future Low-Energy Electronics Technologies (FLEET). A.K. and R. would like to thank Rajib K. Rakshit, Manju Singh, V. R. Reddy, Dr. R. P. Pant, and Dr. Chhemendra Sharma for PLD, XRD, and RSM measurement.

Conflict of Interest

The authors declare no conflict of interest.

Keywords

ferroelectric domains, ferroelectric/superconductor heterostructures, low-pressure mechanical switching

Received: May 22, 2020
Revised: July 31, 2020

---

[1] H. Lu, C.-W. Bark, D. E. De Los Ojos, J. Alcala, C.-B. Eom, G. Catalan, A. Gruverman, *Science* **2012**, *336*, 59.
[2] G. Vats, Y. Bai, D. W. Zhang, J. Juuti, J. Seidel, *Adv. Opt. Mater.* **2019**, *7*, 1800858.
[3] Y. Bai, G. Vats, J. Seidel, H. Jantunen, J. Juuti, *Adv. Mater.* **2018**, *30*, 1803821.
[4] Y. Cao, A. Morozovska, S. V. Kalinin, *Phys. Rev. B* **2017**, *96*, 184109.
[5] K. Kim, J. E. Huber, *J. Eur. Ceram. Soc.* **2015**, *35*, 1459.
[6] D. Edwards, S. Brewer, Y. Cao, S. Jesse, L. Q. Chen, S. V. Kalinin, A. Kumar, N. Bassiri-Gharb, *Adv. Mater. Interfaces* **2016**, *3*, 1500470.
[7] S. M. Yang, A. N. Morozovska, R. Kumar, E. A. Eliseev, Y. Cao, L. Mazet, N. Balke, S. Jesse, R. K. Vasudevan, C. Dubourdieu, *Nat. Phys.* **2017**, *13*, 812.
[8] I. S. Vorotiahin, E. A. Eliseev, Q. Li, S. V. Kalinin, Y. A. Genenko, A. N. Morozovska, *Acta Mater.* **2017**, *137*, 85.
[9] Y. Kim, S. J. Kelly, A. Morozovska, E. K. Rahani, E. Strelcov, E. Eliseev, S. Jesse, M. D. Biegalski, N. Balke, N. Benedek, *Nano Lett.* **2013**, *13*, 4068.
[10] S. Das, B. Wang, Y. Cao, M. R. Cho, Y. J. Shin, S. M. Yang, L. Wang, M. Kim, S. V. Kalinin, L.-Q. Chen, *Nat. Commun.* **2017**, *8*, 615.
[11] L. Ma, W. Chen, Y. Liu, B. Wang, Y. Zheng, *Acta Mater.* **2019**, *158*, 23.
[12] Y. Heo, P. Sharma, Y. Liu, J. Li, J. Seidel, *J. Mater. Chem. C* **2019**, *7*, 12441.
[13] G. Catalan, J. Seidel, R. Ramesh, J. F. Scott, *Rev. Mod. Phys.* **2012**, *84*, 119.
[14] R. Pandey, G. Vats, J. Yun, C. R. Bowen, A. W. Ho-Baillie, J. Seidel, K. T. Butler, S. I. Seok, *Adv. Mater.* **2019**, *31*, 1807376.
[15] G. Vats, S. Patel, A. Chauhan, R. Vaish, *Int. J. Appl. Ceram. Technol.* **2015**, *12*, 765.
[16] G. Vats, J. Peräntie, J. Juuti, J. Seidel, Y. Bai, *Energy Technol.* **2020**, https://doi.org/10.1002/ente.202000500.
[17] R. Ramesh, *Int. Soc. Opt. Photonics Spintron.* **2016**, *9931*, 99312K.
[18] D. Fang, Y. Jiang, S. Li, C. Sun, *Acta Mater.* **2007**, *55*, 5758.
[19] J. Bian, Y. Wang, R. Zhu, L. Wang, B. Yang, J. Wang, D. Zhang, C. Xu, T. Li, D. Viehland, *ACS Appl. Mater. Interfaces* **2019**, *11*, 40758.
[20] E. Guo, R. Roth, S. Das, K. Dörr, *Appl. Phys. Lett.* **2014**, *105*, 012903.
[21] A. Alsubaie, P. Sharma, G. Liu, V. Nagarajan, J. Seidel, *Nanotechnology* **2017**, *28*, 075709.
[22] A. Gómez, J. M. Vila-Fungueiriño, R. Moalla, G. Saint-Girons, J. Gázquez, M. Varela, R. Bachelet, M. Gich, F. Rivadulla, A. Carretero-Genevrier, *Small* **2017**, *13*, 1701614.

[23] P. Sharma, Y. Heo, B. K. Jang, Y. Liu, V. Nagarajan, J. Li, C. H. Yang, J. Seidel, *Adv. Mater. Interfaces* **2016**, *3*, 1600033.
[24] P. Sharma, K. R. Kang, B. K. Jang, C. H. Yang, J. Seidel, *Adv. Electron. Mater.* **2016**, *2*, 1600283.
[25] P. Sharma, K. R. Kang, Y. Liu, B.-K. Jang, J. Li, C.-H. Yang, J. Seidel, *Nanotechnology* **2018**, *29*, 205703.
[26] S. V. Kalinin, S. Jesse, B. J. Rodriguez, E. A. Eliseev, V. Gopalan, A. N. Morozovska, *Appl. Phys. Lett.* **2007**, *90*, 212905.
[27] W. Cao, L. E. Cross, *Jpn. J. Appl. Phys.* **1992**, *31*, 1399.
[28] A. Kumar, D. Barrionuevo, N. Ortega, A. Shukla, S. Shannigrahi, J. Scott, R. S. Katiyar, *Appl. Phys. Lett.* **2015**, *106*, 132901.
[29] G. Vats, S. Kumari, D. K. Pradhan, R. S. Katiyar, V. Ojha, C. R. Bowen, A. Kumar, *J. Magn. Magn. Mater.* **2019**, *473*, 511.
[30] G. Vats, A. Kumar, N. Ortega, C. R. Bowen, R. S. Katiyar, *Energy Environ. Sci.* **2016**, *9*, 2383.
[31] G. Vats, A. Kumar, N. Ortega, C. R. Bowen, R. S. Katiyar, *Energy Environ. Sci.* **2016**, *9*, 1335.
[32] X. Yu, L. Wu, B. Zhang, H. Zhou, Y. Dong, X. Wu, R. Kou, P. Yang, J. Chen, C.-J. Sun, *Phys. Rev. B* **2019**, *100*, 104405.
[33] B. D. Cullity, *Elements of X-Ray Diffraction*, Addison-Wesley Publishing, Boston, MA **1956**.
[34] Z.-X. Ye, Q. Li, Y. Hu, W. Si, P. Johnson, Y. Zhu, *Appl. Phys. Lett.* **2005**, *87*, 122502.
[35] A. Panchwanee, V. Raghavendra Reddy, R. Choudhary, D. Phase, V. Ganesan, A. Gupta, *J. Appl. Phys.* **2019**, *125*, 234102.
[36] B. C. Jeon, D. Lee, M. H. Lee, S. M. Yang, S. C. Chae, T. K. Song, S. D. Bu, J. S. Chung, J. G. Yoon, T. W. Noh, *Adv. Mater.* **2013**, *25*, 5643.
[37] D. Lee, B. C. Jeon, A. Yoon, Y. J. Shin, M. H. Lee, T. K. Song, S. D. Bu, M. Kim, J. S. Chung, J. G. Yoon, *Adv. Mater.* **2014**, *26*, 5005.
[38] T. R. Shrout, S. J. Zhang, *J. Electroceram.* **2007**, *19*, 113.
[39] G. Williamson, W. Hall, *Acta Metall.* **1953**, *1*, 22.
[40] M. Nonnenmacher, M. o'Boyle, H. K. Wickramasinghe, *Appl. Phys. Lett.* **1991**, *58*, 2921.
[41] U. Celano, T. Hantschel, G. Giammaria, R. C. Chintala, T. Conard, H. Bender, W. Vandervorst, *J. Appl. Phys.* **2015**, *117*, 214305.
[42] M. Lantz, S. O'shea, M. Welland, K. Johnson, *Phys. Rev. B* **1997**, *55*, 10776.
[43] D. Maugis, *J. Colloid Interface Sci.* **1992**, *150*, 243.
[44] S. M. Park, B. Wang, S. Das, S. C. Chae, J.-S. Chung, J.-G. Yoon, L.-Q. Chen, S. M. Yang, T. W. Noh, *Nat. Nanotechnol.* **2018**, *13*, 366.
[45] T. Tomita, J. Schilling, L. Chen, B. Veal, H. Claus, *Phys. Rev. Lett.* **2006**, *96*, 077001.
[46] S. T. Hartman, B. Mundet, J.-C. Idrobo, X. Obradors, T. Puig, J. Gázquez, R. Mishra, *Phys. Rev. Mater.* **2019**, *3*, 114806.
[47] M. Tomita, M. Murakami, S. Nariki, K. Sawa, *Supercond. Sci. Technol.* **2002**, *15*, 846.
[48] M. L. Scullin, J. Ravichandran, C. Yu, M. Huijben, J. Seidel, A. Majumdar, R. Ramesh, *Acta Mater.* **2010**, *58*, 457.
[49] M. L. Scullin, C. Yu, M. Huijben, S. Mukerjee, J. Seidel, Q. Zhan, J. Moore, A. Majumdar, R. Ramesh, *Appl. Phys. Lett.* **2008**, *92*, 202113.
[50] E. Fradkin, S. A. Kivelson, *Nat. Phys.* **2012**, *8*, 864.
[51] R. , C. Singh, A. Panchwanee, R. K. Rakshit, M. Singh, V. Reddy, R. J. Choudhary, V. Ojha, A. Kumar, *AIP Adv.* **2020**, *10*, 075206.
[52] R. Ramesh, A. Inam, W. Chan, B. Wilkens, K. Myers, K. Remschnig, D. Hart, J. Tarascon, *Science* **1991**, *252*, 944.
[53] R. Ramesh, T. Sands, V. Keramidas, *Appl. Phys. Lett.* **1993**, *63*, 731.
[54] A. R. West, *Solid State Chemistry and its Applications*, John Wiley & Sons, Hoboken, NJ **2014**.